

SPIN-POLARIZED ELECTRON TRANSPORT IN SINGLE-WALLED CARBON NANOTUBES

NSF Summer Undergraduate Fellowship in Sensor Technologies
Kiran V. Thadani - Physics & Systems Engineering, University of Pennsylvania
Advisor: Dr. A.T. Johnson, Jr.

ABSTRACT

A mounting research effort geared towards miniaturization of electronic devices has led to the emergence of a new field called molecular electronics. A particular type of carbon molecule called the nanotube has been playing an integral role in steering this revolution. Nanotubes are micron-long and nanometer-thick cylindrical shells of carbon that have been found to have excellent electrical and thermal conductivities. Their ability to behave as metals or semiconductors depending on the tube structure has led to their incorporation in nano-scale circuits as diodes, field effect transistors and quantum wires. Conventional electronic devices have exploited the charge of electrons to generate current but there has also been a burgeoning interest in harnessing the intrinsic spin of electrons to produce spin-polarized current- a field that has come to be known as spintronics. My project tries to investigate the transport of spin-polarized electrons through single-walled carbon nanotubes. In a broad sense, my project deals with not only extending contemporary macroscopic technology to the molecular level but also exploring a new conduction mechanism to evaluate the potential of nanotubes as nano-spintronic devices.

1. INTRODUCTION

The drive towards miniaturization and sophistication of electrical devices has been progressing at a relentless pace. Silicon-based microelectronic devices have played an integral role in steering this revolution during the latter part of the last century. Gordon Moore's observation [1] in 1965 of doubled computing capacity in every new silicon chip produced within 18-24 months of the previous one is testimony to the ascendancy of silicon devices in the microelectronics race.

The transition to smaller realms however entails a difference in the underlying physics of materials fabricated at the extreme size scales, and this limitation may curtail further miniaturization of silicon devices. An alternative approach that would avert this limitation might be to exploit entities that 'intrinsically' exist in the smallest realms of matter- individual molecules. Indeed, interest in molecular electronics has been burgeoning since the 1970's, and single-molecule based devices are poised to carry on the legacy of the silicon chip at the nano-scale.

Carbon nanotubes are micron-long and nanometer-thick cylindrical shells of carbon that have been making a pivotal contribution to the advancement of technology at the molecular level. First discovered in 1991 [2], nanotubes have been found to exhibit

incredible strength and elasticity [3] as well as extraordinary thermal [4] and electrical [5] conductivities. These characteristics have led to their incorporation in nano-electronic circuits [6,7,8,9] as well as to applications in other facets of nanotechnology [10,11,12].

Most conventional electrical devices have exploited the *charge* of electrons in the conduction mechanism but there is also a growing interest in harnessing the intrinsic *spin* (up or down) of electrons- a field that has come to be known as *spintronics* [13]. Many of the transport measurements conducted on nanotubes thus far have dealt with the transport of *charge* or the transport of *heat*. This summer, I have been involved in a research effort to investigate the transport of *spin* in these systems. Broadly speaking, my project has tried to probe the potential of nanotubes as spintronic devices.

2. THE MINUSCULE WORLD OF NANOTUBES

2.1 Synthesis and Structure

Carbon nanotubes were first discovered in 1991 [2] by Sumio Iijima at the NEC Corporation in Japan. An electric-arc discharge method involving the evaporation of graphite by subjecting it to an electric field yielded cylindrical shells of about 4—30 nanometers (nm) in diameter. Electron microscopy of these showed coaxial cylindrical shells, one inside the other. These kinds of tubes are therefore called *multi-walled* nanotubes. Later, it was also discovered that adding transition metal catalyst particles [14] to the furnace yielded *single* cylindrical shells of diameter 1-2nm and these are called *single-walled* nanotubes.

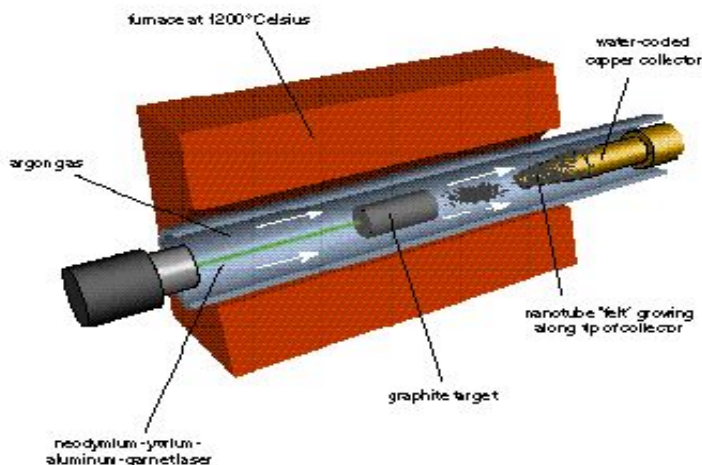


Figure 1: Nanotube growth by laser ablation. Source: Yakobson et al, 1997, [18]

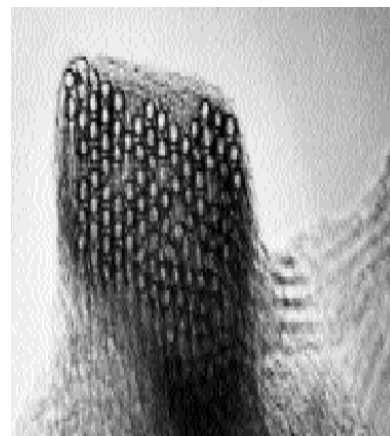


Figure 2: Transmission Electron Microscopy (TEM) image of bundles of carbon nanotubes. Source: Thess et al, 1996, [14]

Several other techniques for synthesizing nanotubes have since been discovered. The most common ones used today are catalyst-assisted laser-ablation [14] (Figure 1) of graphite, which yields nanotube ropes (Figure 2), chemical vapor deposition (CVD) [15] and more recently, HiPCO [16] for bulk production of nanotubes. The principle behind most of these techniques is the evaporation of graphite in the presence of an electric field or laser followed by its condensation resulting in nanotubes. The CVD process involves the deposition of methane or ethylene gas on a catalyst-laden substrate, which facilitates nanotube growth.

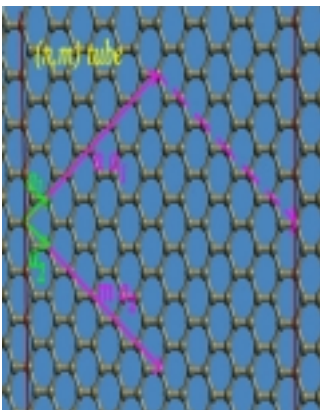


Figure 3: Rolling up a graphene sheet to form a nanotube. Source: Smalley. <http://cnst.rice.edu/>

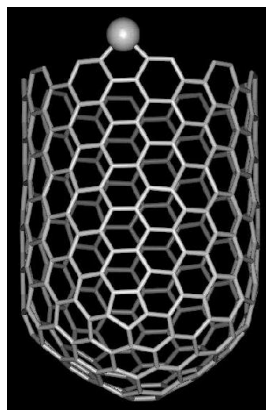


Figure 4: Armchair nanotube. Source: Smalley <http://cnst.rice.edu/>

A nanotube is formed by rolling up a two-dimensional graphene sheet (Figure 3) [17]. The rolling direction is defined by a roll-up vector, which is a linear combination of two vectors, n and m [18]. The structure of the nanotube is labeled as $[n, m]$, where n and m are multiples of the unit vectors, a_1 and a_2 . Nanotubes whose indices satisfy the configuration $m = n$ are called *armchair* nanotubes owing to an armchair replica at the end of the tube (Figure 4). There are also *zigzag* and *chiral* configurations depending on how the graphene sheet is rolled.

2.2 Properties

The rolling direction of the graphene sheet also determines if the tube is metallic or semi-conducting. If the vectors n and m are such that $(n-m) \bmod 3 = 0$, then the tube is metallic; otherwise it is semi-conducting [18]. It has been observed that most of the semi-conducting nanotubes are *p-type*, i.e. the majority of the charge carriers are holes instead of electrons [19]. This has been attributed to the influence of adsorbed impurities that dope [20] the nanotube surface or exposure to oxygen in the air [21]. Experiments have shown that the presence of these impurities can alter the local electronic properties of a semi-conducting nanotube thereby enabling it to behave as a diode [6].

Semiconducting nanotubes have also been fabricated as field effect transistors (TUBEFET's) at room temperature (Figure 5) [7]. The tube is contacted to two electrodes- the source and the drain that complete the circuit. The substrate on which the tube and the electrodes lie acts as a gate. Altering the gate voltage induces the opposite charge in the nanotube thereby affecting its conductivity. A positive gate voltage would thus decrease the conductance of a *p-type* tube while a negative gate voltage would increase it.

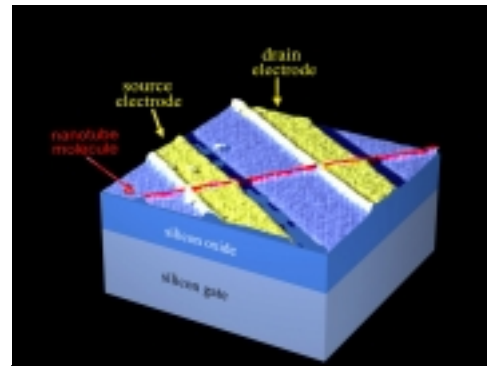


Figure 5: A nanotube transistor. Source: Tans et al, 1998, [7]

Metallic nanotubes have been found to carry current densities of more than 10^9 Ampere/ cm^2 [5]. These high current densities are believed to be attributed to minimal scattering of traversing electrons- that is, to ballistic conductance. In 1-dimensional (1-D) systems like nanotubes, electrons can be scattered back in only one direction as opposed to several directions in 2-D and 3-D systems [22]. Scattering of electrons can occur due to intrinsic defects in the nanotube or due to the emission of phonons at high voltages. At low voltages, electrons do not have sufficient energy to scatter back from defect-scatterers. However, at high voltages, electrons have very high energy and they produce phonons. In order to conserve momentum, the momentum of the phonons has to be balanced by that of the electrons thereby resulting in backward electron scattering. Metallic nanotubes behave as almost perfect 1-D conductors at low voltages.

In addition to their incredible electrical properties, nanotubes are also ideal experimental systems for investigating the transport of electrons in reduced dimensions [23]. Nanotubes belong to a class of 1-D systems called Luttinger liquids. In such systems, electrons move in concert thereby making electron-electron interactions significant. Hence each time an electron is added, the electrostatic potential energy increases by $E_C = e^2/C$ (charging energy). At low temperatures, the thermal energy ($k_B T$) is less than the charging energy (E_C) thereby blocking transport. This has been the basis for nanotube quantum wires [8] and single-electron transistors [24] at low temperatures.

Current progress in nanotube electronics has relied on the manipulation of the *charge* of electrons. The application of an electric field accelerates the electrons and results in electric current. However, there has also been a rising interest in manipulating the *spin* of electrons [25,26]. Spintronics is a class of electronic devices that utilize an external magnetic field instead of an external electric field to maneuver electron flow. Most contemporary spintronic devices [13, 27] have been fabricated on a macroscopic scale but as in conventional microelectronics, there has been a mounting research effort to fabricate these on the molecular scale. My project has tried to investigate the spin-polarization characteristics of electrons tunneling through nanotubes in order to assess their potential for nano-spintronic devices.

3. SPINTRONIC DEVICES

Most atoms have a net magnetic dipole moment because of the orbital motion of their electrons (orbiting electrons constitute current and all currents produce a magnetic field) coupled with the intrinsic spin of electrons [28]. Thus the magnetic moment of each atom in the material is aligned in a particular direction. Ferromagnetic materials are a class of materials constituted of certain regions called *magnetic domains* that have concentrations of parallel-aligned atoms. While all the atoms *inside* a domain are aligned in one direction, the domain *itself* may be misaligned with respect to other domains.

When an external magnetic field is applied, a majority of the magnetic domains become aligned in the direction of the magnetic field and the material is then said to be polarized. The degree of polarization (P) is given by $P = (N_{up} - N_{down}) / (N_{up} + N_{down})$, where N_{up} is the number of electron spins that are polarized parallel to the magnetic field and N_{down} is the number of electron spins that are anti-parallel to it [13].

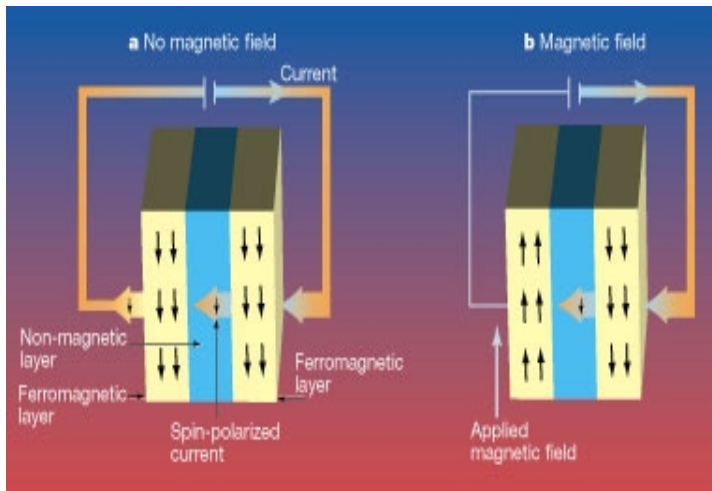


Figure 6: Giant Magneto Resistance (GMR) observed in ferromagnetic layers. Even in the absence of an external magnetic field, there is an intrinsic spin-polarization in the ferromagnetic layers thereby yielding current. In the presence of a magnetic field, there is greater spin-polarization in both layers. Parallel electron-spin alignment in the two layers gives lower resistance while anti-parallel alignment yields higher resistance. Source: *Nature*, 2000, [27]

The principle behind the operation of most spintronic devices is called giant magneto resistance (GMR) [13]. GMR is a quantum mechanical effect observed when two or more ferromagnetic layers are separated by non-magnetic layers (Figure 6). When an external magnetic field is applied, the domains in each ferromagnetic layer become aligned in a particular direction thereby resulting in a net alignment of each layer. The degree of

polarization in each layer depends on the nature of ferromagnetic material used while the *simultaneity* in alignment or misalignment of spins in subsequent layers depends on whether the constituent materials of the layers are the same or different. Parallel alignment of two ferromagnetic layers gives a lower resistance while anti-parallel alignment yields higher resistance. Thus the resistance of the circuit can be controlled by an external magnetic field.



Figure 7: Spintronics in computer hard drives.
Source: *Nature*, 2000, [27]

The setup of ferromagnetic layers discussed above is often called a *spin-valve* [13]. Typically, the device is constructed so that only one of the ferromagnetic layers is sensitive to the external magnetic field. This sensitive layer then acts as a valve-control because it is the sole regulator of the relative alignment of the two layers. A spin-valve can also act as a ‘memory device’ [27] because the valve-control can retain its alignment even after the device has been switched off. Such an application can be found in computer hard-drives (Figure 7) that store data permanently in thin magnetic films.

Spintronic devices are essentially multifunctional [26,29] because the spin current has to be controlled by both electric and magnetic fields. The magnetic field is responsible for *polarizing* the spins of the charge carriers while the electric field is responsible for *moving* the carriers. One of the most intriguing applications of spintronics is revealed in quantum computing [30]. Quantum computing relies on ‘quantum bits’ or ‘qubits’, which are coherent super-positions of the binary digits, 0 and 1. Spintronics, which is based entirely on fundamental phenomena such as electron and nuclear spins in atoms may hold the key to scaling up qubits that are essential for generating an elaborate computing instrument.

The biggest challenge [26] for spintronic devices lies in establishing *coherent* spin transport [25]. Spin-current through two ferromagnetic materials placed next to each other, can be inhibited by three potential spin-scattering sites that can induce incoherence: (1) the source of spin-polarized carriers, (2) the interface between the two layers [29] and (3) the destination layer. The addition of magnetic dopants [31] to semiconductor layers as well as the application of certain optical techniques have yielded some success in mitigating the chances of scattering but the search for an efficient spintronic system continues.

4. THE APPROACH TO NANOTUBE SPINTRONICS

4.1 Strategy of the Experiments

The goal of my project has been to investigate the transport properties of spin-polarized electrons in single-walled carbon nanotubes. In order to measure certain characteristics such as electrical, magnetic or super-conducting properties of a nanotube, one has to first contact the nanotube with metallic leads. The nature of the metallic leads depends on the type of measurement being undertaken. For example, gold leads are used for electrical measurements on nanotubes because of the high conductance of gold. There are three possible sources of resistance in a nanotube circuit: (1) resistance of the nanotube itself, (2) resistance of the metallic leads, and (3) contact resistance at the nanotube-lead interface. The observed resistance in the circuit is a combination of these and it is difficult to isolate the contribution of the nanotube resistance in such a measurement. Hence, it becomes imperative to minimize the potential contribution from elements in the *environment* of the nanotube as opposed to the contribution from its intrinsic *system*.

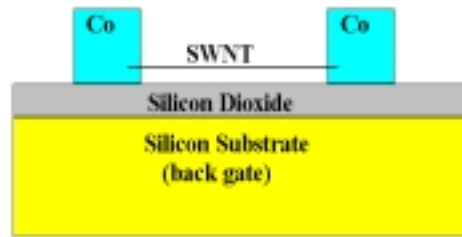


Figure 8: Schematic diagram of single-walled carbon nanotube contacted with ferromagnetic cobalt leads. The cobalt leads are 20nm thick while the nanotube is 1-2nm in diameter.

In my experiments, I have contacted the nanotube with cobalt leads because cobalt is ferromagnetic (Figure 8). The leads are a source of spin-polarized electrons for the contacted nanotube [32]. When an external magnetic field is applied, a majority of electrons in each of the ferromagnetic leads are polarized in either the up- or down spins. Parallel polarization in the leads would yield lower resistance in the circuit while anti-parallel polarization would yield higher resistance. The dependence of resistance on the relative polarization of the leads might also be supplemented by spin-flip or spin-scattering *inside* the nanotube and at the nanotube-lead interface. Spin-scattering lengths in metals [33] and semiconductors [34] have been found to be much longer than the respective elastic scattering lengths; this project will seek to investigate this difference in the nanotube system.

4.2 Experimental Techniques and Equipment

The approach undertaken for preparing and measuring the nanotube samples was four-fold:

- i. **Growing** single-walled carbon nanotubes on a silicon substrate by a procedure called chemical vapor deposition (CVD) [15]
- ii. **Locating** the nanotubes on the substrate using a tapping-mode Atomic Force Microscope (AFM)
- iii. **Designing** a pattern of cobalt leads using a Scanning Electron Microscope (SEM) by a process called electron-beam (e-beam) lithography and subsequent deposition of cobalt using an evaporator
- iv. **Measuring** the nanotube sample

The nanotubes are grown on a degenerately doped silicon substrate that is coated with a 100nm thick insulating silicon-oxide layer to prevent the conducting silicon from shorting the electrodes that will contact the nanotube [35]. Optical lithography is used to fabricate gold markers on the silicon surface to facilitate the mapping of the exact locations of the nanotubes (Figure 9).

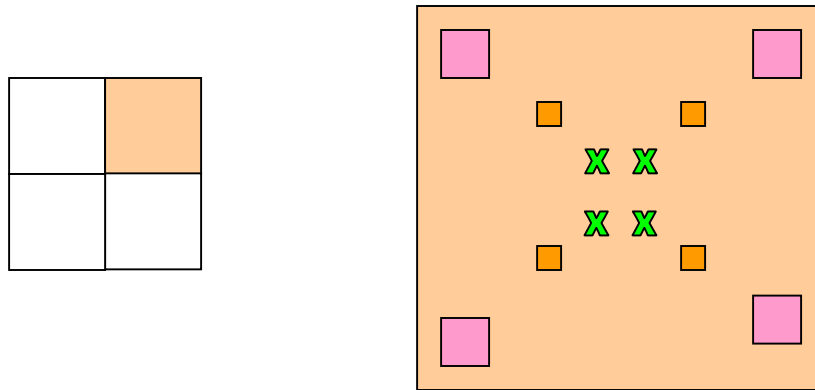


Figure 9: The diagram on the left pictorially represents the four areas of the chip. The diagram on the right is a detailed map of the gold markers in the shaded area of the left diagram. A similar pattern is repeated on the other corners (not shaded) of the chip as well. The distance between the outer pink markers is 860 microns; between the orange markers, 86 microns and between the green crosses, 40 microns.

When an AFM scan of the chip is taken, the area between the green crosses is probed and the nanotubes are located with respect to each of these green markers.

The first step in growing nanotubes is to prepare a catalyst solution by mixing fused alumina and ferric nitrate followed by dissolving the paste in ethanol [36]. The catalyst is sonicated for 30 minutes to facilitate pulverization of the big catalyst particles in the solution. Meanwhile, the silicon chip on which the nanotubes will be grown is thoroughly cleaned with acetone. This is followed by the deposition of the sonicated catalyst on the chip (Figure 10).

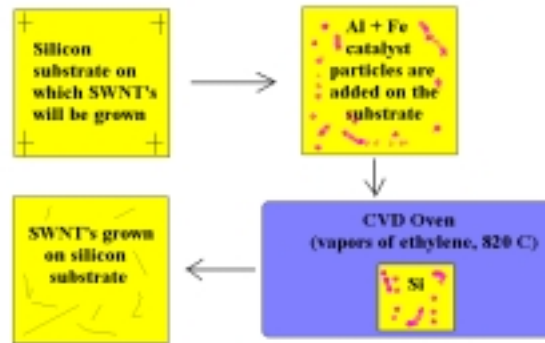


Figure 10: Schematic diagram of CVD- growth of nanotubes. The nanotubes are grown on a Si substrate. Catalyst (pink) is deposited on the substrate and then the chip is inserted inside a CVD oven where it is subjected to ethylene gas at a temperature of 820 C. Nanotubes (thin green lines) are then grown on the chip. Note: The green lines on the last element of the flow chart are not drawn to scale

The catalyst-laden substrate is then inserted inside a CVD oven (Figure 10) and hydrogen, argon and ethylene gases are allowed to flow into the chamber for 12 minutes. Thereafter, the ethylene gas is turned off while the oven is heated to 820⁰ C, a process that usually takes 45-60 minutes. Subsequently, the ethylene gas is turned on again for 10 minutes. At this time, nanotubes grow on the substrate. Consequently, the ethylene flow is stopped and the oven is switched off to cool the chip, while hydrogen and argon gases continue to flow. The hydrogen gas ‘protects’ the nanotubes from oxidation by reacting with any oxygen that may seep into the chamber. It takes about 70-90 minutes for the temperature to drop to 400⁰C, and the hydrogen flow is then stopped. After about 2-3 hours when the temperature falls to below 150⁰C, argon is turned off and the samples are removed from the oven.

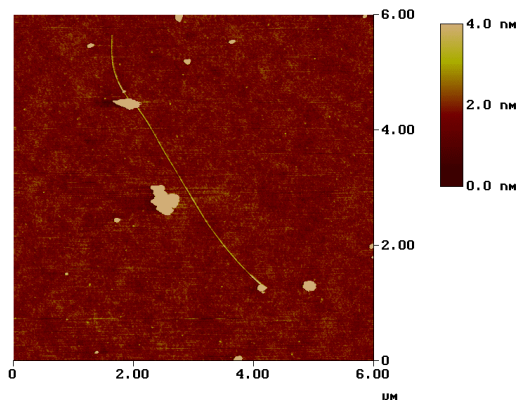


Figure 11: AFM image of a nanotube emerging from a catalyst particle (yellow spot at the bottom right of image) lying on a silicon substrate (red)

Once the nanotubes are grown on the substrate, their exact locations are imaged (Figure 11) with a Digital Instruments “Dimension 3000” AFM. The topography of the surface is determined as a function of the force between the cantilever tip and the substrate. The nanotubes are first located on 20µm scans of areas demarcated by certain markers (see green crosses in Figure 9). This facilitates their precise mapping when leads are designed to contact them.

After all four regions of the chip have been scanned with the AFM, leads are designed using lithography software. These designs of the contacting leads are then translated into patterns on the chip (Figures 12, 13) using a Scanning Electron Microscope (SEM). First, a PMMA (Poly-methyl- meth-acrylate) *resist* is spun on the chip at 3000 rpm for 45 seconds giving a layer thickness of 100–500nm. Following this, the chip is subjected to *electron-beam lithography*, which involves the bombardment of the PMMA polymer by electrons. Thereafter, the sample is *developed* by being dipped for 45 seconds in IPA (Iso-propyl-alcohol) and MIBK (Methyl-iso-butyl-ketone). Subsequently, cobalt is *evaporated* on the sample and *liftoff* is undertaken to remove cobalt from all areas of the chip external to the lead patterns.

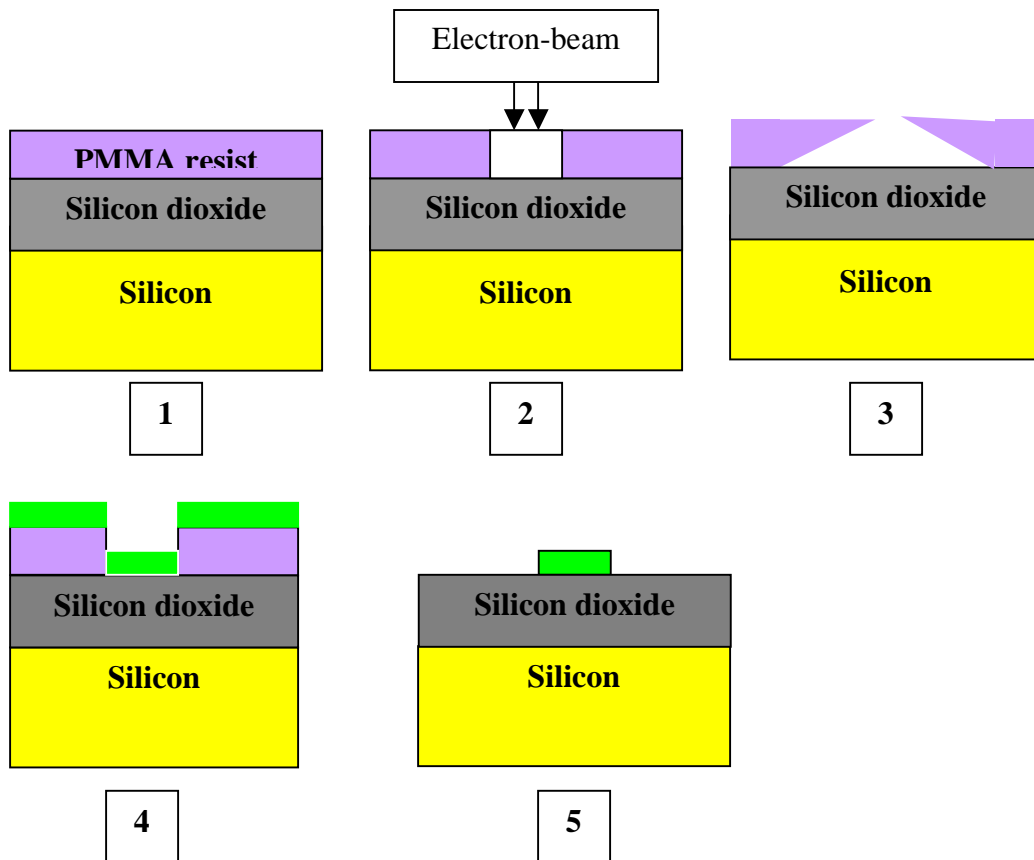


Figure 12: Steps involved in contacting the nanotube with cobalt leads.
 (1) Depositing PMMA resist on chip
 (2) Electron-beam lithography on PMMA resist creates patterns on the surface
 (3) Developing the chip in IPA + MIBK (undercut profile)
 (4) Evaporating cobalt metal (green)
 (5) Liftoff removes resist and cobalt metal from all other areas of the chip

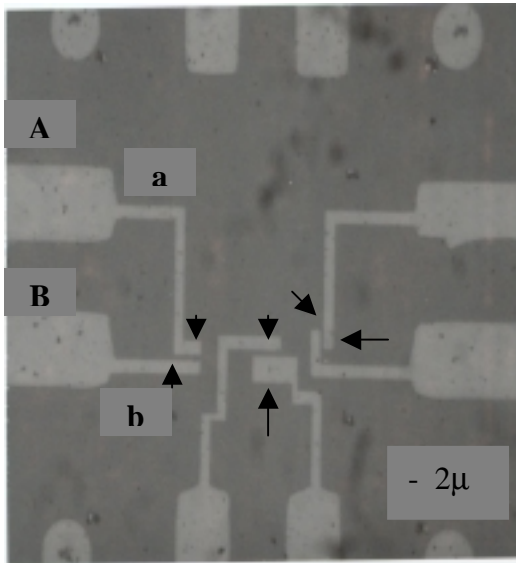


Figure 13: A Polaroid image of cobalt leads (white) fabricated by e-beam lithography. This photograph was taken under an optical microscope. The thickness of the big leads (see leads A, B) emerging from the edges is 10 microns while the thinner leads (a, b) emerging from the big leads are 1-2 microns thick. It is the thinner leads (a, b) that directly contact the nanotube. The nanotubes cannot be seen on this photograph because of its large scale. However, the pairs of arrows point at the gaps between the thinner leads where the nanotubes lie, contacted. In order to see the nanotubes after they have been contacted, an AFM scan of each of the gaps is taken (see Figure 14 below)

Following this procedure, AFM scans of the surface are taken again to verify that the nanotubes have indeed been contacted (Figure 14).

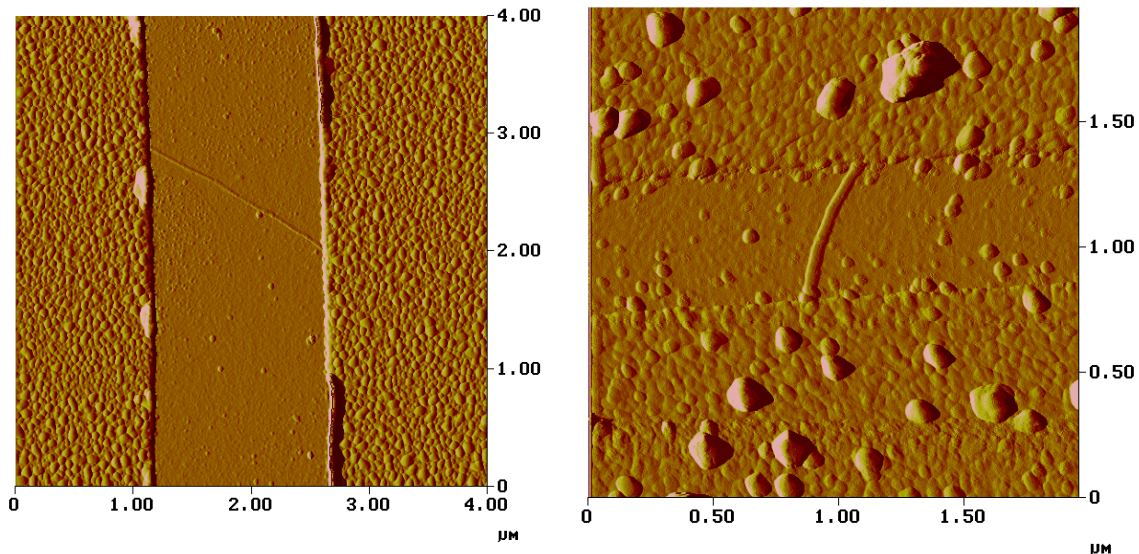


Figure 14: AFM images of nanotubes contacted with cobalt leads. The nanotubes are 1-2 nm in diameter while the cobalt leads are 20nm thick. (Left) The nanotube is contacted with cobalt leads on the right and left edges (rough surface). (Right) The nanotube is contacted with cobalt leads on the top and bottom edges. The pink blob-like pieces on the surface are catalyst particles that are 30nm thick.

After the nanotubes have been contacted, they are ready to be measured. The next section discusses the experiments undertaken as well as the corresponding results attained for the contacted nanotubes.

5. MEASUREMENTS AND RESULTS

5.1 Preliminary Measurements At Room Temperature

Preliminary measurements were taken at room temperature to measure the resistance of the contacted nanotubes in order to test for their metallic or semi-conducting nature. This data was obtained from an instrument called the probe station, which consists of macroscopic probes that contact the cobalt pads on the chip and record the current and voltage across the nanotube sample. The typical resistance of CVD-grown metallic nanotubes is 20-60 kOhms ($k\Omega$) while that for semi-conducting nanotubes is 1-2 MOhms ($M\Omega$) [37]. Hence, from the I-V curves obtained, a reasonable interpretation was made for the metallic or semi-conducting behavior of the nanotubes. Shown below are data for some of the contacted nanotubes (Figure 15).

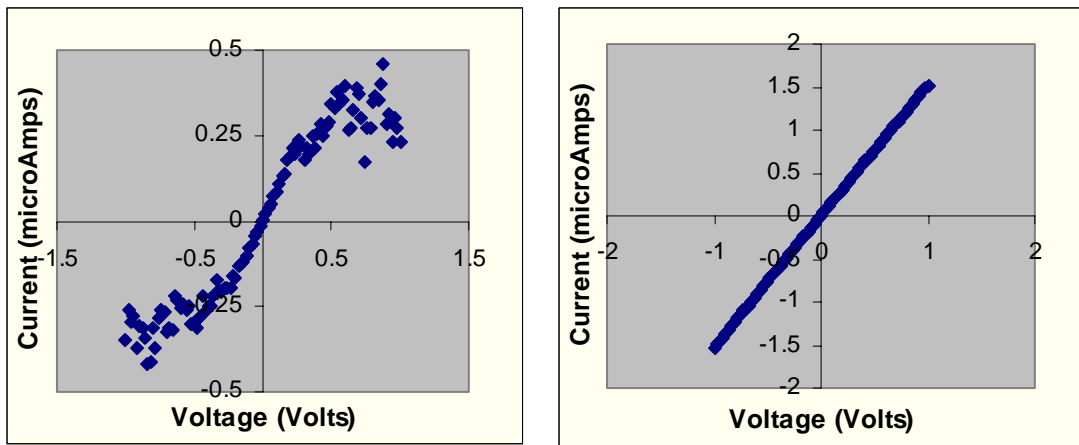


Figure 15: (Left) I-V for a semiconducting nanotube. The resistance is about $2M\Omega$. (Right) I-V for a metallic nanotube. The resistance is about $660 k\Omega$

From the above data, it was seen that the resistance of the semi-conducting nanotubes was about 2-3 Mohm ($M\Omega$) and that of the metallic ones was about 660 kOhm ($k\Omega$). While the resistance of the semi-conducting nanotubes was within the expected range, the resistance of the metallic nanotubes was found to be extraordinarily high. This high resistance may be attributed to either defects inside the nanotube or to defective cobalt metal. The defects in CVD-grown nanotubes produce localized states that couple well to the electrodes [37], thereby reducing the contribution of the contact resistance. Also, CVD-grown nanotubes have a lower resistance compared to laser-grown nanotubes [37]; it seems unlikely therefore that nanotube defects are responsible for the high resistance.

It is speculated that the major contribution to this high resistance stems from bad metal and cobalt oxidation is believed to be the primary reason for this. The same piece of cobalt metal was used for two consecutive evaporations on different samples. The metal was evaporated the second time within a week of the first evaporation. While the cobalt for the samples evaporated upon in the first week had a silver sheen, the metal on the

samples in the second week had a pink color. This might be evidence for the oxidation of the metal while it lay exposed to air in the week-long span between the two evaporations.

After these preliminary room temperature measurements, the chips were mounted in gold-plated chip carriers and wire bonded with silver epoxy. The semi-conducting nanotubes were experimented on further with a conducting-tip AFM while the metallic nanotubes were prepared for measurements at low temperatures (77 K). The results from these sets of experiments will be discussed in the next few sections.

5.2 Conducting-Tip AFM Measurements Of Semi-Conducting Nanotubes

Conducting-tip AFM experiments were undertaken on a few nanotubes that had been found to be semi-conducting at room temperature (Figure 16). Semi-conducting nanotubes have been found to be typically *p-type* owing to the influence of oxygen in the air [21], which sucks out the electrons from the tube. However, in the conducting-tip AFM measurements of my samples, a surprisingly *different* observation was made: cobalt-contacted nanotubes were found to be *n-type* semiconductors.

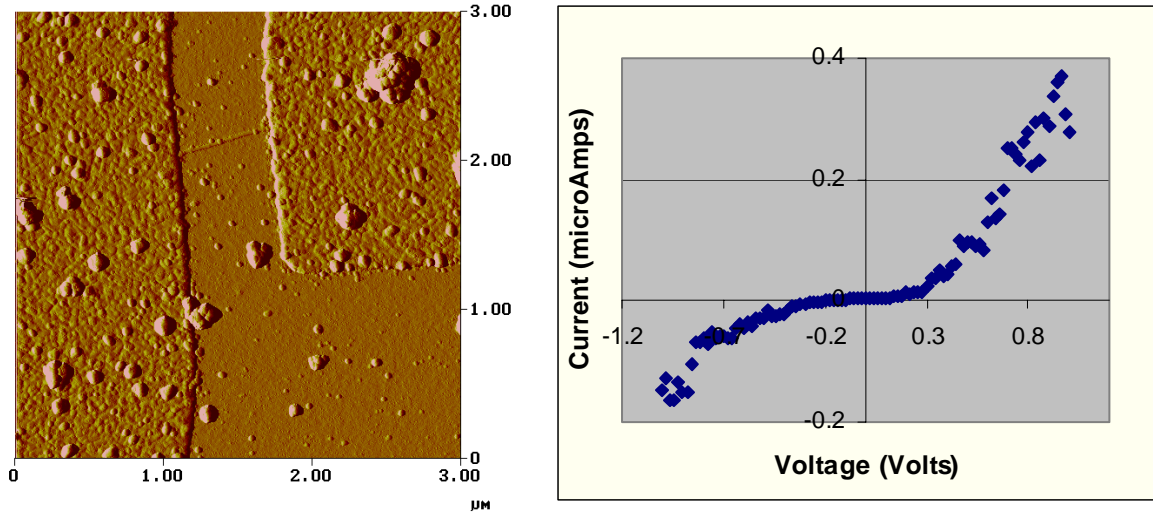


Figure 16: The image on the left is an AFM image of a contacted nanotube that was found to be semi-conducting at room temperature. The plot on the right is the I-V curve at room temperature for this nanotube.

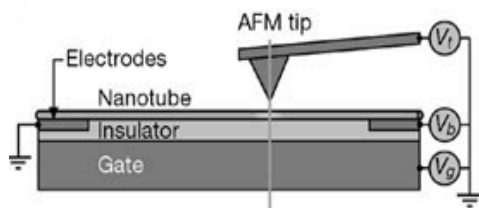
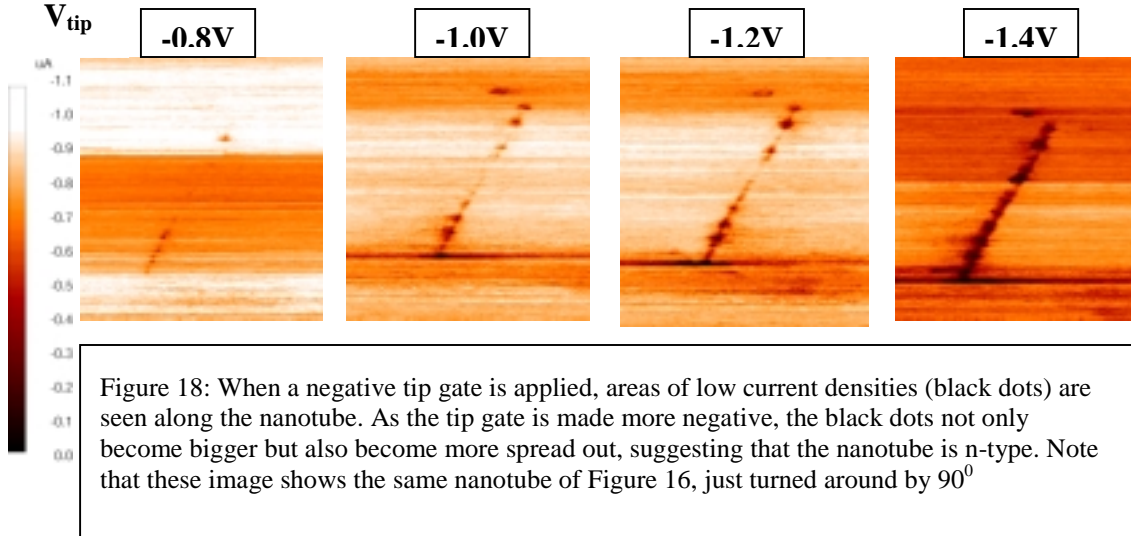


Figure 17: Setup of conducting-tip AFM. Source: Tans et al, 2000, [38]

In CT-AFM, a voltage is applied at the AFM tip (Figure 17). Unlike a back-gate voltage (applied on the substrate) that has a *global* effect by altering the charge density *everywhere* in the circuit, the tip voltage has a *local* effect by inducing charge locally on the nanotube thereby shifting the Fermi level of the system [37, 38].

The resistance of the circuit is thus recorded as a function of the tip voltage as well as the tip position. A higher tip voltage will have the same effect as a decreasing tip-surface distance owing to the higher electrostatic coupling between the tip and tube and vice versa [39].



When a negative tip gate voltage was applied, black dots were observed along the nanotube (Figure 18). These black dots represent areas of low current density. This is the first indication of the n-type behavior of the nanotube, for a negative tip gate voltage induces more holes and depletes more electrons in the nanotube. A decreasing current density owing to depletion of electrons implies that the majority of the charge carriers must be electrons and hence the nanotube must be n-type.

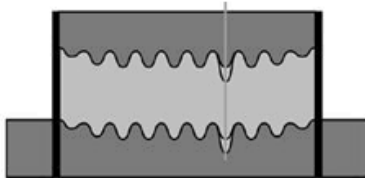
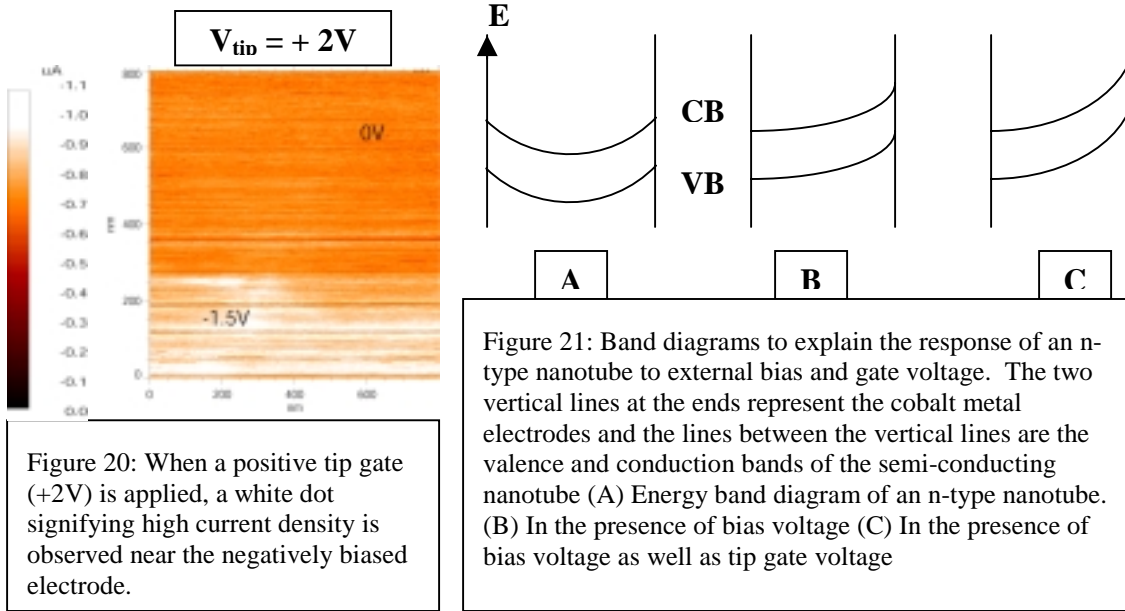


Figure 19: The wiggles in the valence band and conduction band. As the negative gate voltage is increased, more energy is available to remove electrons that are deep down in the wiggles resulting in greater electron depletion. Source: Tans et al, 2000, [38]

As the tip gate voltage was made more negative, the black dots were found to become not only *bigger* but also more *spread out* along the length of the nanotube. The increase in size of the dot corresponding to an increase in negative tip gate voltage might be attributed to the greater extent of electron depletion in that *local* region of the nanotube [37]. The spreading out of the dots may be ascribed to the greater energy available to deplete the electrons settled deep down in the uneven wiggles of the conduction band (Figure 19).

It was also observed that when a positive tip gate voltage was applied, a higher current density was obtained near the negatively biased electrode (Figure 20). This is attributed to the truncation of the depletion region near the negatively biased electrode owing to a shift in the conduction band of the nanotube upon the application of the tip gate voltage.



It is unclear why cobalt-contacted nanotubes are n-type but it is speculated that there might be some cobalt interaction with carbon to form carbides that might induce the n-type characteristics.

Figure 21 shows the hypothetical energy band diagrams for an n-type nanotube. Figure 21A shows the band diagram of the nanotube when no bias and gate are applied. The vertical lines at the right and left ends represent the cobalt metal electrodes while the lines between them represent the valence (VB) and conduction bands (CB) of the semi-conducting nanotube. The bands are aligned so that the Fermi energy of the metal electrodes equilibrates with the Fermi level of the nanotube.

The free electrons in the metal electrodes go across the metal-tube interface and result in a net negative charge at the interface. The n-type nanotube also has a majority of electrons as charge carriers and hence due to Coulomb repulsion between electrons, there is higher energy at the metal-tube interface and lesser energy in the middle of the nanotube. That is why the bands are ‘pinned’ to the metal at the interface and they ‘sag’ in the middle of the nanotube (Figure 21A). Due to the difference in work functions between the nanotube and the metal electrodes, a Schotky barrier is induced at the metal-tube interface [19].

When an external bias (according to Figure 21, negative bias on right electrode) is applied (Figure 21B), the Schotky barrier at one of the electrodes (in this case, the left electrode) becomes forward biased while the barrier at the other electrode (in this case, the right electrode) becomes reverse biased. When a voltage is applied to the AFM tip (Fig 21C), the gating action shortens the depletion region near the reverse biased electrode as the bands become steeper at that electrode.

5.3 Observation Of A Nanotube Diode At Room Temperature

One of the contacted nanotubes was found to exhibit diode-like behavior at room temperature. The I-V curves, unlike those for metallic or semi-conducting nanotubes, were found to be highly asymmetric (Figure 22).

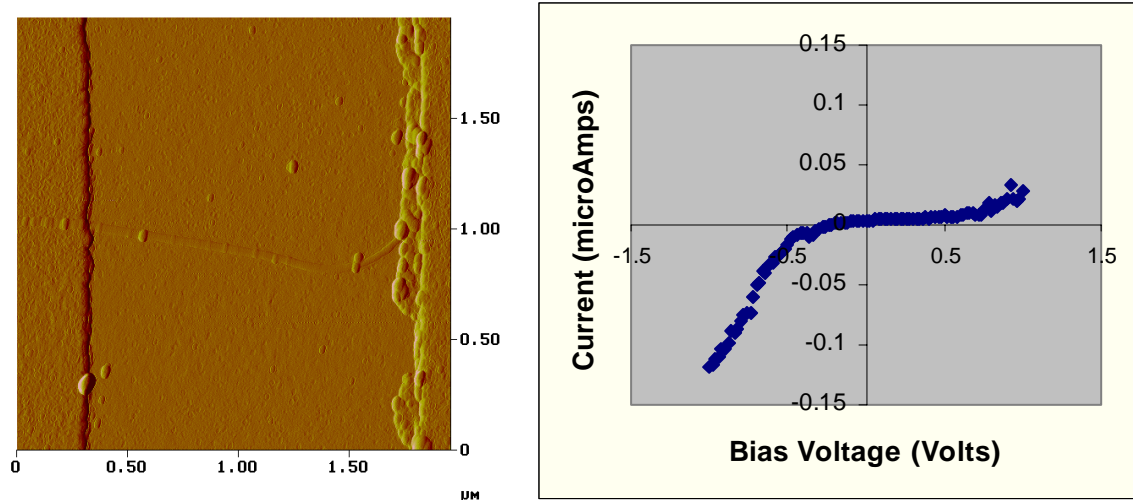


Figure 22: (left) AFM image of the nanotube contacted to two cobalt electrodes on the right and left. The dark lines near the right and left edges of the image are the boundaries of the 20-nm thick cobalt leads that flank the nanotube. The impurities on the right side are believed to alter the electronic properties of the nanotube and cause it to exhibit diode-like characteristics
(right) The I-V curve obtained for the nanotube diode at room temperature.

It has been shown previously [6] that the presence of an impurity on a semi-conducting nanotube can locally alter its electronic properties and cause it to behave like a diode (Figure 23). It was shown that when a bias was applied between B and C, the I-V was symmetric as expected for a semi-conducting nanotube. However, when a bias was applied between A and B, the I-V was found to be asymmetric owing to the presence of an n-type impurity dopant near lead A. As a result, high current was observed when lead A was biased negatively with respect to lead B and almost no current was observed when lead A was biased positively with respect to lead B.

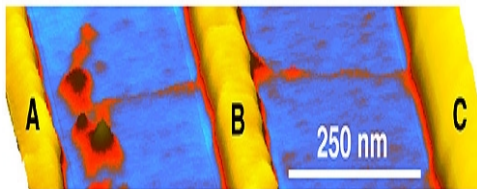


Figure 23: Nanotube diode. Source: Antonov et al., 1999, [6]

In the nanotube sample measured in my experiment also, it is speculated that the diode behavior may be attributed to the influence of impurities present at the right end of the nanotube (Figure 22). The bias was applied at the left cobalt electrode while the right

electrode was grounded. It is seen from the I-V curve (Figure 22) that there is an increasing current at negative bias and almost no current at positive bias. This suggests that the part of the nanotube closer to the left electrode might be *more negative or more n-type* than the right part. This may be ascribed to two possibilities:

- a. The cobalt leads might indeed be making the nanotube n-type as shown by the conducting-tip AFM experiments discussed in the previous section. If this were the case, then the impurities at the right end would be *p-type* dopants and hence would induce an n-p junction (Figure 24a). As a result, there would be forward bias when the left electrode is negatively biased with respect to the right electrode and reverse bias when it is positively biased with respect to the right one.

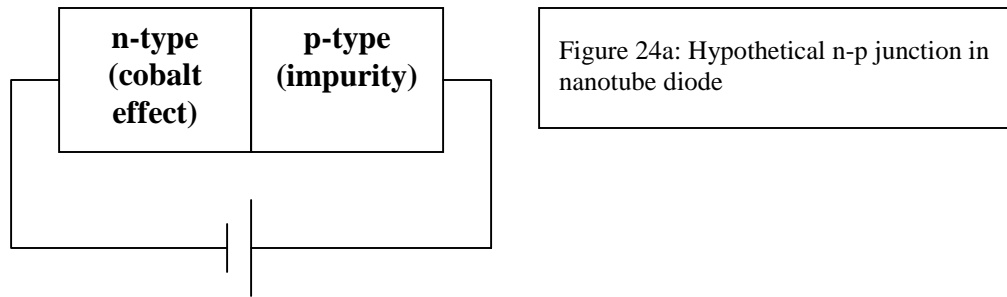


Figure 24a: Hypothetical n-p junction in nanotube diode

- b. The nanotube might be *p-type* but the impurities may be even more *positive or p-type* thereby inducing a p-p⁺ junction (Figure 24b). Thus, a negative bias at the left electrode would correspond to forward bias producing more current while a positive bias at this electrode would correspond to reverse bias producing no current.

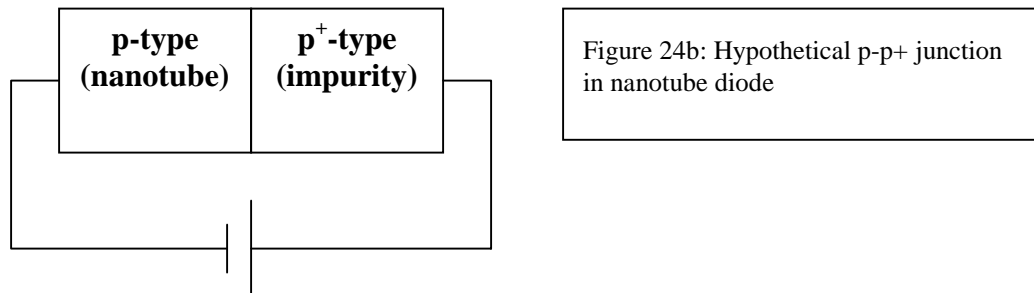


Figure 24b: Hypothetical p-p+ junction in nanotube diode

5.4 Low Temperature (77K) Measurements Of Metallic Nanotubes

Metallic nanotube samples (Figure 25) were inserted into a measuring stick at 77 K. The samples were first cooled overnight in liquid nitrogen and thereafter, incorporated in the circuit at the low temperature.

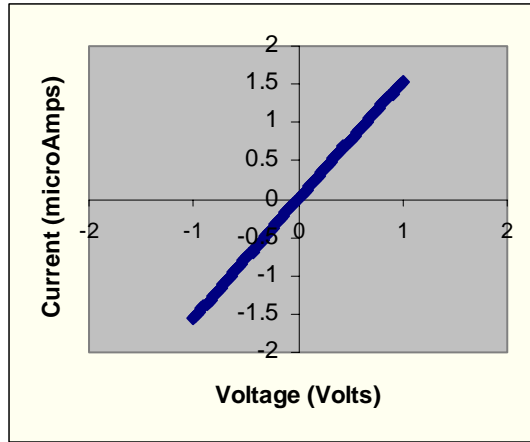
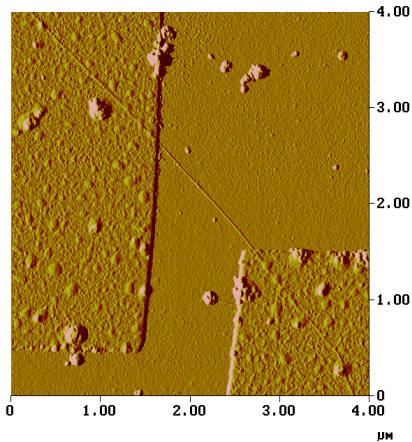


Figure 25: The image on the left is an AFM image of a contacted nanotube that was found to be metallic at room temperature. The plot on the right is the I-V curve at room temperature for this nanotube.

To measure the resistance of the sample, the circuit was first current biased (Figure 26); that is, a current was passed through the sample and then, the voltage change across it was observed. This was achieved by inserting a resistor of high magnitude (about 100 MΩ) in series with the sample. As a result, most of the applied current passed through the nanotube sample whose resistance with respect to the resistor became insignificant. By reading off the voltage across the sample, a somewhat accurate calculation could be made for the resistance of the nanotube.

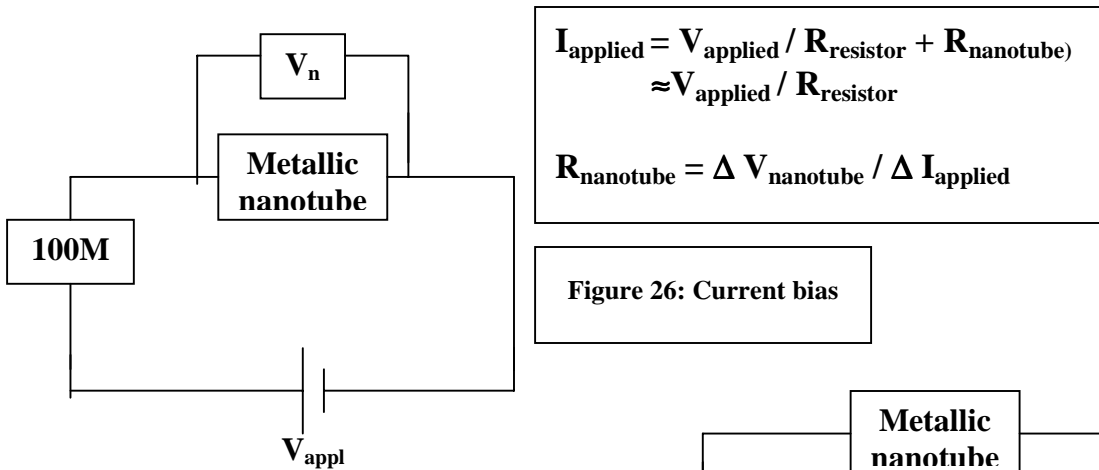
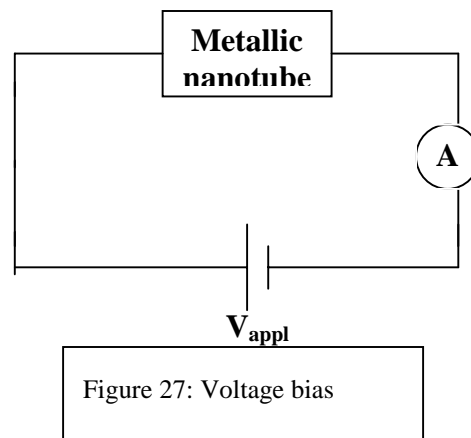


Figure 26: Current bias

Subsequently, the circuit was voltage biased (Figure 27); that is, a voltage was applied across the sample and the current change was observed. The circuit was voltage biased because the voltage-bias approach is preferable to the current-bias approach for high resistance samples and as discussed earlier, the metallic nanotubes in the sample subset exhibited extraordinarily high resistances.



Gate voltage sweeps from -10V to $+10\text{V}$ were taken at different bias voltages. For metallic nanotubes, the current through the circuit is expected to be independent of gate voltage [8]. However, for my metallic samples, an unexpected dip was observed as the gate voltage approached 0 (Figure 28)

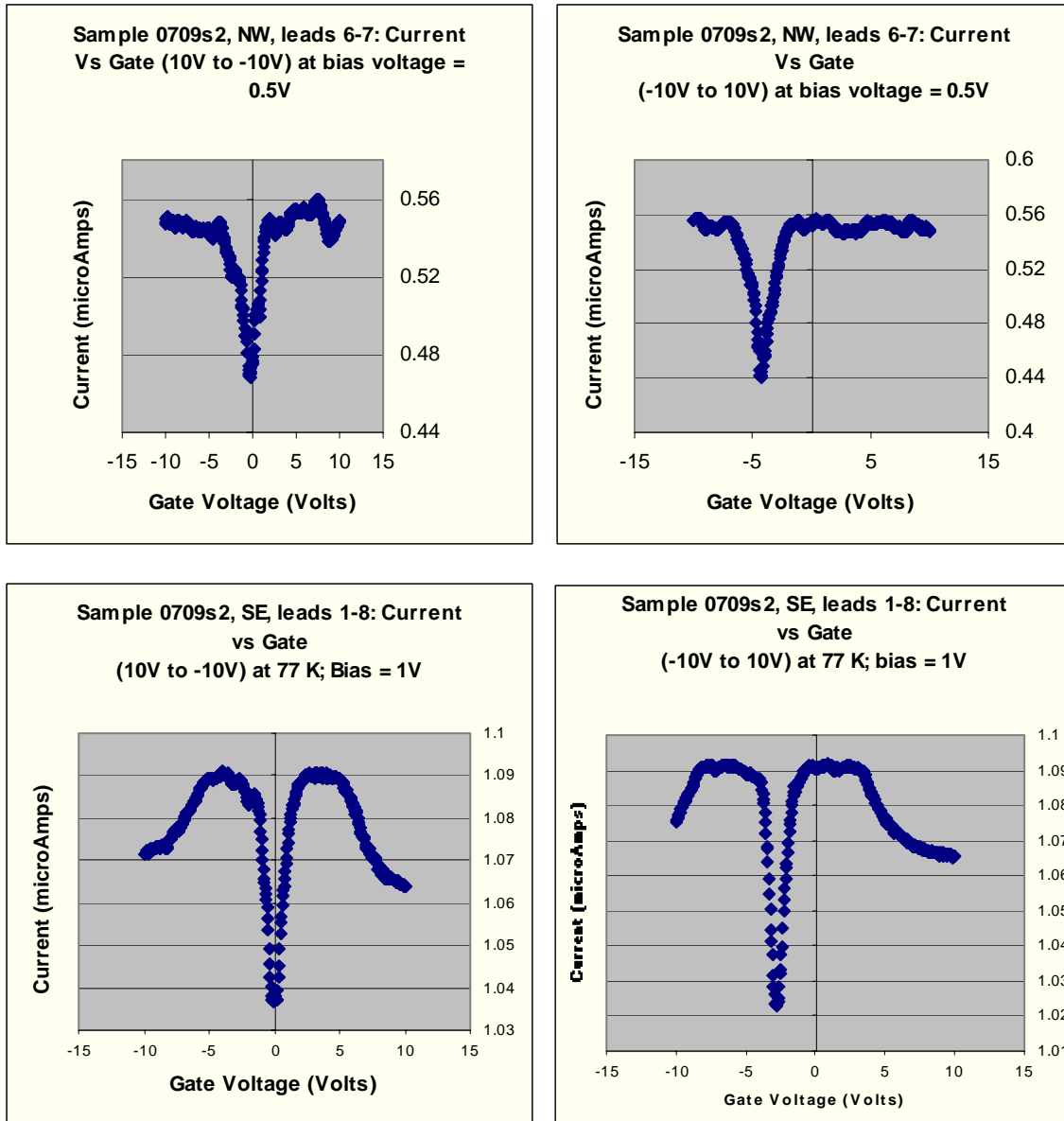


Figure 28: Current Vs Gate Voltage for two metallic samples at 77 K. The plots at the top show the dependence of current on gate voltage for the first metallic sample. The bias voltage is 0.5 V. The top left graph shows the plot for a gate sweep from 10V to -10V and the right graph shows the plot for a gate sweep from -10V to 10V. The plots at the bottom show the corresponding plots for the second metallic sample at bias voltage of 1V

Two interesting points are noted about the above data for the two samples.

- a) The current is not always independent of the gate voltage. Instead of seeing a flat curve with no slope, a current ‘dip’ is seen at around 0 gate voltage.
- b) For both samples, it is observed that when the gate voltage is swept from +10V to –10V, the current dip is observed at 0 gate voltage whereas when the gate voltage is swept from –10V to +10V, the current dip is observed at a slightly negative voltage.

These results are unexpected and further analysis would be required to explain them.

6. CONCLUSIONS

The experiments done this summer were directed towards investigating spin-polarized electron transport in single-walled carbon nanotubes. The approach undertaken was four-fold: nanotubes were first synthesized by chemical vapor deposition, then located on the substrate by AFM followed by electron-beam lithography to contact them with cobalt leads and finally measured.

The measurements were first taken at room temperature to determine the semi-conducting or metallic characteristics of the nanotubes. Following this preliminary analysis, the electronic properties of the semi-conducting nanotubes were probed further by conducting-tip AFM experiments. It was found that cobalt-contacted nanotubes exhibit n-type behavior unlike the typical *p-type* characteristics observed in contemporary experiments involving other metal leads. Room temperature experiments also showed diode-like behavior in one of the nanotube samples.

The electronic properties of metallic nanotubes were investigated at low temperatures (77 K). The dependence of current on the gate voltage was found to be unexpectedly prominent. Further analysis would be required to understand this aberrant behavior.

7. FUTURE APPROACH & RECOMMENDATIONS

The experiments undertaken this summer have revealed some interesting characteristics about nanotube interaction with ferromagnetic cobalt leads. Future experiments may involve measurements of these samples in magnetic field to investigate the dependence of magneto-resistance on the applied magnetic field. Such an experiment was done on multi-walled nanotubes [32] a few years ago and hysteric resistance peaks were observed owing to spin-polarized injection from the leads to the nanotubes. About 14% of electrons were found to retain their polarization throughout the nanotube length.

Based on the results of experiments done this summer, it would be highly probable for any prospective magnetic field experiments on single-walled nanotubes to entail the dependence of resistance on the nanotube-lead interaction in addition to the intrinsic spin-scattering properties of the nanotube medium. In order to isolate electron-transport *inside*

the nanotube from transport at the tube-lead *interface*, it will be essential to have ferromagnetic leads with low resistance. To facilitate this, it is recommended that evaporation of the same metal on different samples be avoided.

Future experiments on spin-polarized transport in nanotubes may also be motivated by an effort to completely *decouple* the charge and spin of electrons. In current spintronic devices, spin transport is an *addendum* to charge transport; however, spin-polarized transport has not yet been demonstrated *independently* of charge-transport. If continuing research efforts in one-dimensional molecular-scale systems like nanotubes demonstrate their potential as media conducive for spin-transport, then the pace of spintronic technology could progress by leaps and bounds and the dream of nano-spintronics might become a reality.

8. ACKNOWLEDGEMENTS

I would like to thank Dr. A.T. Charlie Johnson for his excellent mentorship throughout the project as well as Marko Radosavljevic, Marcus Freitag and the Johnson research group for their invaluable guidance and assistance in my experiments. I am grateful to the National Science Foundation for supporting my research project through the NSF-REU grant. I would also like to acknowledge the University Scholars Program at the University of Pennsylvania for their encouragement and support in this project.

9. REFERENCES:

1. Intel Corporation, <http://www.intel.com/intel/museum/25anniv/hof/moore.htm>
2. S. Iijima, Helical microtubules of graphitic carbon, *Nature*, 354 (1991) 56-58.
3. P. Poncharal, Z.L. Wang, D. Ugarte and W.A. de Heer, Electrostatic deflections and electromechanical resonances of carbon nanotubes, *Science*, 283 (1999) 1513-1516.
4. J. Hone, B. Batlogg, Z. Benes, A.T. Johnson and J.E. Fischer, Quantized phonon spectrum of single-wall carbon nanotubes, *Science*, 289 (2000) 1730-1733.
5. S. Frank, P. Poncharal, Z.L. Wang and W.A. de Heer, Carbon nanotube quantum resistors, *Science*, 280 (1998) 1744-1746.
6. R.D. Antonov and A.T. Johnson, Subband population in a single-wall carbon nanotube diode, *Phys. Rev. Lett.*, 83 (1999) 3274-3276.
7. S.J. Tans, A.R.M. Verschueren and C. Dekker, Room-temperature transistor based on a single carbon nanotube, *Nature*, 393 (1998) 49-52.
8. S.J. Tans, A.R.M. Verschueren and C. Dekker, Individual single-wall nanotubes as quantum wires, *Nature*, 386 (1997) 474-477.
9. M.S. Fuhrer et al, Crossed nanotube junctions, *Science*, 288 (2000) 494-497.
10. H. Dai, J.H. Hafner, A.G. Rinzler, D.T. Colbert and R.E. Smalley, Nanotubes as nanoprobe in scanning probe microscopy, *Nature*, 384 (1996) 147-150.
11. J. Lefebvre, J.F. Lynch, M. Llaguno, M. Radosavljevic and A.T. Johnson, Single-wall carbon nanotube circuits assembled with an atomic force microscope, *Appl. Phys. Lett.*, 75 (1999) 3014-3016.
12. J. Lefebvre, M. Radosavljevic and A.T. Johnson, Fabrication of nanometer size gaps in a metallic wire, *Appl. Phys. Lett.*, 76 (2000) 3828-3830.

13. G.A. Prinz, Magnetoelectronics, *Science*, 282 (1998) 1660-1663.
14. A. Thess, R. Lee, P. Nikolaev et al., Crystalline ropes of metallic carbon nanotubes, *Science*, 273 (1996) 483-487.
15. J. Kong, H.T. Soh, A.M. Cassell, C.F. Quate and H. Dai, Synthesis of individual single-walled carbon nanotubes on patterned silicon wafers, *Nature*, 395 (1998) 878-881.
16. P. Nikolaev, M.J. Bronikowski, R.K. Bradley et al, Gas-phase catalytic growth of single-walled carbon nanotubes from carbon monoxide, *Chem. Phys. Lett.*, 313 (1999),-.
17. M.S. Dresselhaus, G. Dresselhaus and P. Eklund, *Science of Fullerenes and Carbon Nanotubes*, San Diego: Academic Press, 1996.
18. B.I. Yakobson and R.E. Smalley, Fullerene Nanotubes: C_{1,000,000} and Beyond, *American Scientist*, 85 (1997) 324-337.
19. S. M. Sze, *Semiconductor Devices*, Wiley, New York, 1985.
20. R.S. Lee, H.J. Kim, J.E. Fischer et al., Transport properties of a potassium-doped single-wall carbon nanotube rope, *Phys. Rev. B*, 61 (2000) 4526-4529.
21. P.G. Collins, K. Bradley, M. Ishigami and A. Zettl, Extreme oxygen sensitivity of electronic properties of carbon nanotubes, *Science*, 287 (2000) 1801-1804.
22. P.L. McEuen, Single-wall carbon nanotubes, *Physics World*, June (2000) 31-36.
23. M. Bockrath, D.H. Cobden, J. Lu et al., Luttinger-liquid behaviour in carbon nanotubes, *Nature*, 397 (1999) 598-601.
24. M. Bockrath, D.H. Cobden, P.L. McEuen et al., Single-electron transport in ropes of carbon nanotubes, *Science*, 275 (1997) 1922-1925.
25. I. Malajovich, J.J. Berry, N. Samarth and D.D. Awschalom, Persistent sourcing of coherent spins for multifunctional semiconductor spintronics, *Nature*, 411 (2001) 770-772.
26. M. Roukes, Electronics in a spin, *Nature*, 411 (2001) 747-748.
27. P. Ball, Meet the spin doctors, *Nature*, 404 (2000) 918-920.
28. J. Bernstein, P. Fishbane and S. Gasiorowicz, *Modern Physics*, Prentice Hall, New Jersey, 2000.
29. V.P. LaBella, D.W. Bullock, Z. Ding et al., Spatially resolved spin-injection probability for Gallium Arsenide, *Science*, 292 (2001) 1518-1521.
30. J.A. Gupta, R. Knobel, N. Samarth and D.D. Awschalom, Ultrafast manipulation of electron spin coherence, *Science*, 292 (2001) 2458-2461.
31. H. Ohno, Making nonmagnetic semiconductors ferromagnetic, *Science*, 281 (1998) 951-956.
32. K. Tsukagoshi, B.W. Alphenaar and H. Ago, Coherent transport of electron spin in a ferromagnetically contacted carbon nanotube, *Nature*, 401 (1999) 572-574.
33. M. Johnson and R.H. Silsbee, Interfacial charge-spin-coupling-injection and detection of spin, *Phys. Rev. Lett.*, 55 (1985) 1790-1793.
34. J.M. Kikkawa and D.D. Awschalom, Resonant spin amplification in n-type GaAs, *Phys. Rev. Lett.*, 80 (1998) 4313-4316.
35. R. Antonov, PhD Thesis, Department of Physics, University of Pennsylvania (1999).
36. M. Radosavljevic, PhD Thesis, Department of Physics, University of Pennsylvania (2001).

37. M. Freitag, M. Radosavljevic, Y. Zhou, A.T. Johnson and W.F. Smith, Controlled creation of a carbon nanotube diode by a scanned gate, -, - (2001).
38. S.J. Tans and C. Dekker, Molecular transistors: Potential modulations along carbon nanotubes, *Nature*, 404 (2000) 834-835.
39. M. Bockrath, W. Liang, D. Bozovic, J. Hafner, C. Lieber, M. Tinkham, and H. Park, Resonant electron scattering by defects in single-walled carbon nanotubes, *Science*, 291 (2001) 283-285.